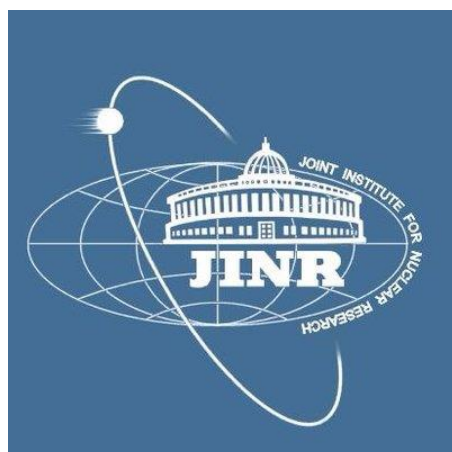# Joint Institute for Nuclear Research

Flerov Laboratory of Nuclear Reactions

Summer School Report

Multinucleon transfer: an overview about ^{160}Gd + ^{186}W reaction

Supervisors:
Prof. Alexander V. Karpov
Prof. Eduard M. Kozulin

Candidates:
Salvatore Spinosa
Nazarena Tortorelli

Contents

Multinucleon transfer: an overview about $^{160}Gd +^{186}W$ reaction

August 2, 2018

Abstract   About thirty years ago, multinucleon transfer reactions involving actinide nuclei targets were considered as a possible mean to produce new neutron-rich isotopes of heavy and superheavy (SH) nuclei. The search for mechanisms to produce SH elements was triggered by the observation that the cross sections for production of SH elements via fusion reactions were found to decrease rapidly with increasing atomic numbers of reacting nuclei. Furthermore, it was found that the yields for fusion-evaporation in the case of near and above actinide nuclei targets depend strongly on the choice of the projectile nucleus. By studying the distribution of binary reaction products formed in low-energy dissipative collisions between heavy ions it is possible to highlight nuclear structure effects. [1]

For elements with $Z > 100$ only neutron-deficient isotopes have been synthesized with fusion-evaporation reactions. However, the "northeast" area of the nuclear map cannot be reached in the fusion, fission, or fragmentation processes. Therefore, multinucleon transfer can represents a possible pathway. This process seems to be the only one known allowing us to produce and explore neutron-rich heavy nuclei near or inside the island of stability. Furthermore, shell effects may give a gain in the yields of heavy neutron-rich nuclei formed in multinucleon transfer reactions.

1   Introduction to multinucleon transfer theory

1.1   Different types of multinucleon transfer reactions

The description of residual nucleus fragments formation is shown schematically in the next figure:

The first type of reaction in figure is the deep inelastic collision, in this case happens that two nuclei collide with grazing angle changing energy and few nucleons. The main features are:

- The collision is binary with projectile like fragment (PLF) and target like fragments (TLF) in the exit channel.

- Angular distributions of the fragments are dependent on charge product $Z_p Z_t$ of the projectile and target.

- Angular distributions are correlated to the net mass and nucleons exchange and to the kinetic energy loss.

- Mass and charge distributions of the fragments are bimodal and centred around the projcctile and target mass and charge.

- Another main feature is the large amount of kinetic energy loss in a collision. Final total kinetic energies can be as low as those corresponding to the coulomb repulsion of highly deformed fission fragments. [3]
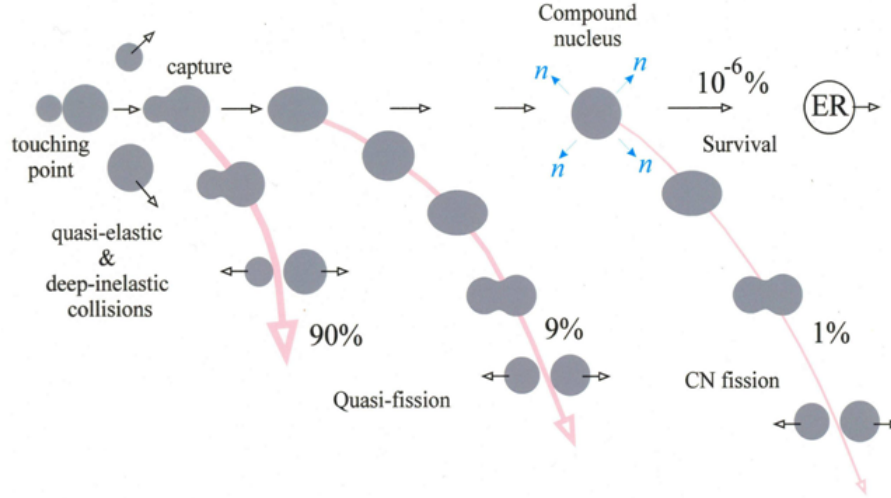
Figure 1: Schematic picture of superheavy nucleus formation

In the second reaction the interacting nuclei evolve in two body system configurations: the quasi fission reactions. In this case happens that, after dynamic deformation and exchange by nucleons, two touching heavy nuclei may re-separate into PLF and TLF without formation of compound nucleus. [4]

The quasi fission is called inverse quasi fission if, after the projectile and the target interacting, many nucleons go from lighter to higher fragment. This process is realized when the nuclei are far away to the shell closure.

The inverse quasi fission mainly leads to the formation of asymmetric fragments, that relates to an influence of the shell structure of the driving potential (deep valley caused by the double shell closure Z=82 and N=126 – double magic lead) on nucleon rearrangement between primary fragments. Instead, in the case of so called normal quasi fission, it happens exchange of few nucleons from lighter to higher interacting fragments and this process leads to the formation of symmetric fragments.

1.2 How to explain the multinucleon transfert: a theoretical model.

We want to explain the main nucleon transfer processes and we needed to a model and we use a multidimensional dynamical approach based on Langevin equations.

The Langevin-type approach allows one to obtain a rather complete information on nuclear dynamics itself as well as to study the characteristics of primary and final reaction products.

This model has eight degrees of freedom that describe a system of two colliding nuclei to have numerically solved equations. [5] Four of them define the nuclear shape:

- The distance between the oscillator centres (elongation) is $r = z_2 - z_1$ (z_1 and z_2 barycentre coordinates), which for separated nuclei is approximately the distance between centres of masses of the nuclei.

- Two independent ellipsoidal deformations δ_1 and δ_2 of the two parts of the system, defined as $\delta i = a_i/b_i - 1$.

- The mass asymmetry $\eta_A = (A_2 - A_1)/(A_1 + A_2)$, where A_1 and A_2 are the masses (volumes) of the left ($z < 0$) and right ($z > 0$) parts of the system, respectively.
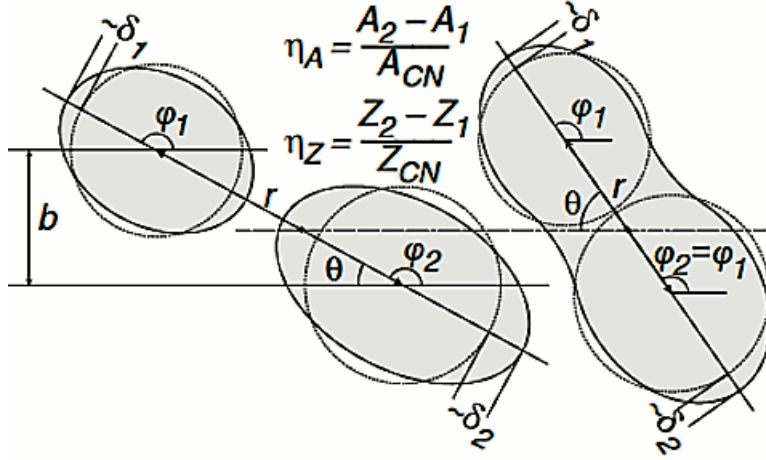
Figure 2: Schematic view of the nuclear degrees of freedom.

- The neck parameter ε is referred from the shape smoothing between the centres z_i. The smaller ε is, the thickener neck is at fixed values of the other parameters. To better description the entrance and exit channel shapes should be taken in to account.

Thus, the model has four degrees of freedom (r, δ_1, δ_2, and η_A) determining the shape of the nuclear system.

- To account for formation of nuclei with different atomic numbers, there is an additional variable — the charge asymmetry η_Z. $\eta_Z = (Z_2 - Z_1)/(Z_2 + Z_1)$, where Z_1 and Z_2 are the charges of the left and right parts of the system, respectively. This degree of freedom is necessary for analysis of transfer reactions with the formation of different isotopes of a given element.

- Additionally, two angles $\varphi_{1,2}$ of rotation of the nuclei and the angle θ between the symmetry axis and the beam direction are considered as independent variables.

Thus, in total, the model has eight degrees of freedom shown schematically in Fig.2 and unified by sequent Langevin equations system:

$$\dot{q_i} = \sum_j \mu_{ij} p_j \tag{1}$$

$$\dot{p_i} = t(\frac{\partial S}{\partial q_i})_{E_{tot}} - \sum_{j,k} \gamma_{ij} \mu_{jk} p_k + \sum_j \theta_{ij} \xi_j(t) \tag{2}$$

where and $q_i = \{r, \delta_1, \delta_2, \eta_A, \eta_Z, \theta, \varphi_1, \varphi_2\}$ $p = \{p_r, p_{\delta_1}, p_{\delta_2}, p_{\eta_A}, p_{\eta_Z}, L, l_1, l_2\}$ are collective degrees of freedom and their conjugate momenta, correspondingly. S is the entropy of excited system, $\mu_{ij} = [m_{ij}]^{-1}$ is the inverse inertia tensor, γ_{ij} is the friction tensor, θ_{ij} are the amplitudes of the random force. The terms in the second equation represent correspondingly the driving, friction and random forces.

A collision schematically begins with the projectile and target approach at a given impact parameter (b) for certain centre-of-mass energy. The calculations are terminated when in the mass centre system, the products are formed and separated again by the initial distance. The obtained solution is a trajectory in multidimensional space of the collective degrees of freedom that carries complete information about a single collision.

4

Numerical solution of the Langevin equations starts from the approaching stage of collision when the target and projectile are separated by $50fm$ and terminates when two reaction products are formed and separated again by approximately $50fm$ distance.

Each trajectory provides full information about a single collision, such as charges and masses of primary (excited) reaction products, their kinetic energies, scattering angles, reaction time, etc. To study the characteristics of final fragments we use the statistical model of de-excitation of an excited rotating nucleus. In this approach, the differential cross sections are calculated as.

$$\frac{d^4\sigma}{dZdAdEd\Omega}(Z, A, E, \theta) = \int\limits_{0}^{b_{max}} \frac{\Delta N(b, Z, A, E, \theta)}{N_{tot}(b)} \frac{bdb}{\Delta Z\Delta A\Delta Esin\theta\Delta\theta} \tag{3}$$

where N is a number of trajectories in specific mass, charge, energy, and angle bins and N_{tot} is the total number of simulated trajectories for each impact parameter. Any single, double, or triple differential cross section can be obtained by integration of Eq. (3). [6]

2 Chapter 2: Experimental set-up

2.1 CORSET

The spectrometer consists of two identical TOF arms, which measure the velocities of both fragments of reactions, and several V – E telescopes, which measure the mass and the energy of only one fragment of the binary process. Each TOF arm contains start and stop detectors based on MCPs, while each V – E telescope comprises two MCP detectors with an electrostatic mirror and a semiconductor detector (Fig.3).
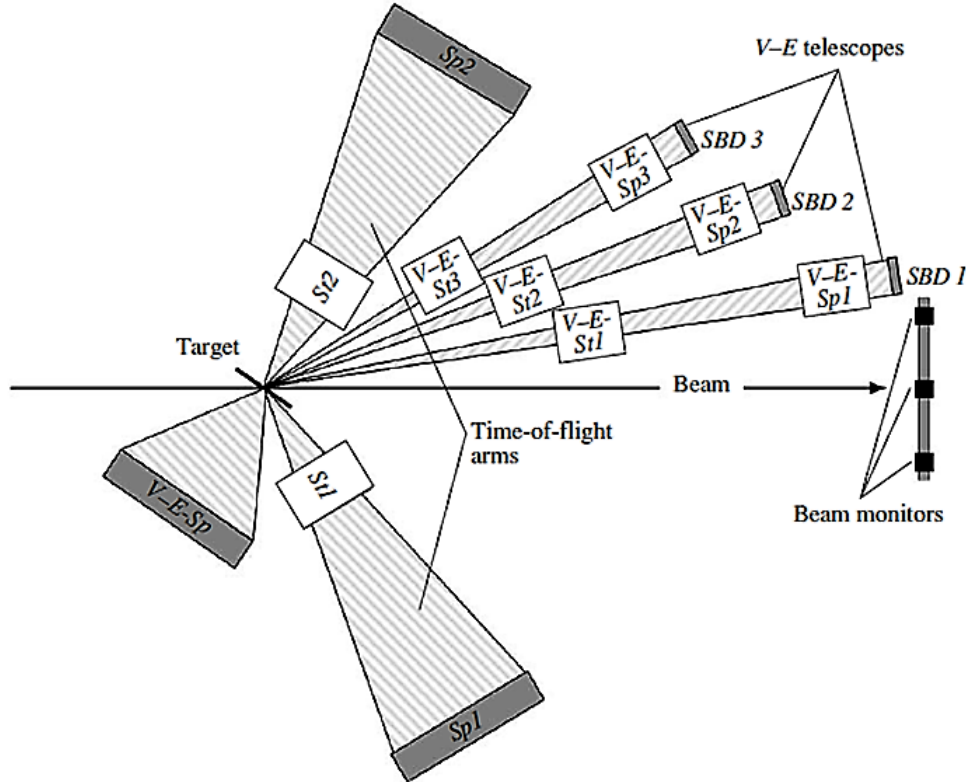
Figure 3: Layout of the detectors in the CORSET spectrometer

Now we are interested to understand how we can analyse the principal channels of heavy ions reactions: elastic and inelastic scattering, deep inelastic collision, quasi fission and fusion fission.

To understand the dynamics of the reaction is important to estimate the contribute of each reaction. To measure the reactions. contribute we must analyse the binary fragments and the residual evaporation.

Counting on the CORSET apparatus, the binary products of the nuclear reactions can be detected using different methods:

- measuring the energy of the two fragments (2E)

- measuring the velocity of the two fragments (2E)

- measuring velocity and energy of a fragment (V-E)

- measuring velocity and energy of each fragment (2E-2V)

Referred to last method, it is important to mark that, although in one side it gives more information, in other side it could be applied with a semiconductor detector, these detectors have a low geometric efficiency because of their small area superconducting. In principle we can use detectors with bigger area sensitivity, to increase the sensitivity but the price would begin too much and because this kind of detector requires to adjust the pulse height defect and the number of the emitted neutrons be introduced.

Speaking about the 2E method, it is possible use ionization spark chambers having a much better energy resolution η_Z on than semiconductor detectors, but these are not suitable in presence of charged particle beam due to a considerable increase in the background level and a high ionization produced by the interaction between gas and bombarding particles.

Referring to the 2V method, the determination of mass and energy values are referred to primary fragments, because the neutron emission is isotropic in the rest frame of the reaction fragment and the mean velocity of the fragment after neutron evaporation is virtually unaltered. For measurement with 2V method it is necessary to have a good time resolution for the system, so the timing detector should be thickness to make the velocity lost negligible during passing through the detector.

The limit of this detector is that at least two foils are used in a start detector to isolate the gas volume from the vacuum region of the reaction chamber, but it happens an high energy loss so a detectors based on micro-channels plates (MCPs) with a resolution time of 100 ps can be used but these detectors in combination with the fill-gas detectors product worsening of resolution; thus, it is necessary enhance the distance between start and MCP detector, so we need of an enhance of the dimension of the set-up.

To examine the neutron, γ -rays and light ions emission, and to avoid the re-scattering of the just detected particles, a minimum volume of the material must be placed on the path of particles from the target to the detector, consequently it happens a decrease in the overall dimensions of the time-of-flight (TOF) spectrometer and a decrease in its flight paths so its mass and energy resolutions deteriorate. So, the best choice is put a stop detector that is composed by an MCP after a position sensitive detector. [7]

2.2 Energy calibration and measure of thickness mylar foil

In this section we shall discuss the calibration of a position-sensitive detector and the how-to determinate the thickness of a foil.

2.2.1 Energy calibration

In a spectrum the position (channel number) for each peak was carefully located, and the pulse height was determined with reference to a precision pulse generator connected throughout the measurements as shown in next Fig.4.

The important feature of these curves is linear relation between ions mass and energy in the fission fragments range

$$E = Ax + B$$

where x and E are the pulse height and ion energy, respectively, and A and B are constants for ions of a given mass. In the range of masses and energies of fission fragments, the coefficient A is approximately linearly dependent on the ion mass. The value of B parameter depends on the nucleus analysed hence, it is sufficiently accurate to introduce the assumption that B also varies linearly with ion mass. Thus, we arrive at a general form for the calibration of the energy solid state detector for fission fragments
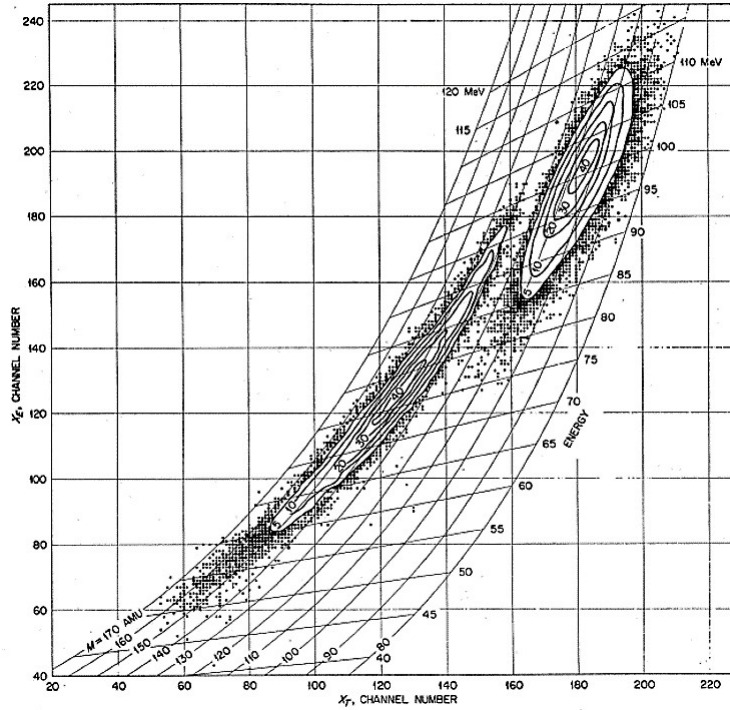
$$E = (a + a'M)x + (b + b'M)$$

7

Figure 4: Two-parameter energy, time-of-fight correlation data for ^{252}Cf spontaneous fission fragments.

where a, a', b, and b' are constants for a detector operated under constant conditions. The equation was then used in the analysis of the energy, time-of-fight correlation data to determine fragment masses and energies. In practice, the constants may be determined in terms of channel number, providing only that the pulse analysis system is linear. Thus, no reference to absolute pulse height is necessary, and the pulse points need be used only for checks of stability and linearity, and for intercalibration among successive runs. [8]

2.2.2 Thickness foil

Now we want to examine the thickness of the mylar foil by using a triple of α source: ^{233}U, ^{238}Pu and ^{239}Pu. The energies and the branching ratio associate of each element are: $4824, 4MeV$ with $84, 4$, $5155, 8MeV$ with $73, 0\%$ and $5499, 1MeV$ with $71, 0\%$.

The chamber is composed by a start detector sitting in front of the source separated by a mylar foil. The chamber reaches a pression of $10^{-2}mbarr$ by the vacuum system, in this way the α are slow down only by the foil without considering the air in the chamber. Subsequently, are measured two emission spectra respectively with and without foil to measure the energy lost with foil presence. The exit of this chamber (the signal measured by the detector inside) is connected to an amplificator and after to the electronic acquisition system. The data analysis was made by the Origin software used to obtain a gaussian fit for each peak in the spectra, the FWHM. Comparing the FWHM values for spectra without foil with the energy peaks in channel we found the conversion factor to convert the channel in energy (spectra calibration in energy).
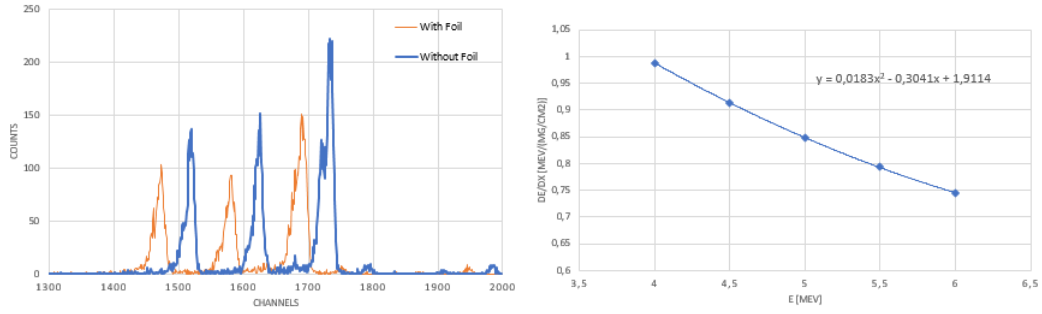
Figure 5: The figure on the left shows with and without foil spectra energy, on the right the polynomial fit for energy lost for path unit.
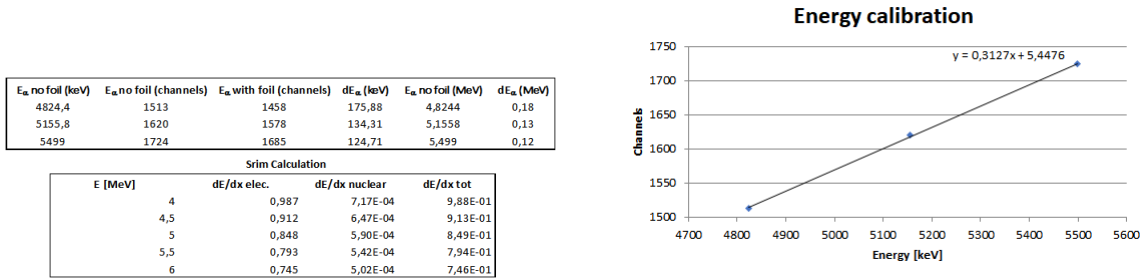

E_α no foil (keV)	E_α no foil (channels)	E_α with foil (channels)	dE_α (keV)	E_α no foil (MeV)	dE_α (MeV)
4824,4	1513	1458	175,88	4,8244	0,18
5155,8	1620	1578	134,31	5,1558	0,13
5499	1724	1685	124,71	5,499	0,12

Srim Calculation			
E [MeV]	dE/dx elec.	dE/dx nuclear	dE/dx tot
4	0,987	7,17E-04	9,88E-01
4,5	0,912	6,47E-04	9,13E-01
5	0,848	5,90E-04	8,49E-01
5,5	0,793	5,42E-04	7,94E-01
6	0,745	5,02E-04	7,46E-01

Figure 6: Energy calibration and Srim calculation.

After, using Srim software, fixing an energetic range $(4 - 6 MeV)$, with the help of a polynomial fit (Fig.5 right) was obtained the formula for energy lost for path unit dE/dx which has a parabolic dependence with energy

$$\frac{dE}{dx} = b_0 + b_1 E + b_2 E^2$$

where b_0, b_1 e b_2 are constants obtained by the fit.

In the end, noted FWHM values in both cases (peaks spectra with and without foil) the energy lost referred to each particle was estimated and divided by dE/dx to obtain the thickness foil (dx $[mg/cm^2]$) for each peak

$$dx = \frac{dE}{b_0 + b_1 E + b_2 E^2} \tag{4}$$

Averaging for three peaks the thickness calculated was

$$dx = 173, 76 \, \mu g/cm^2 \tag{5}$$

3 Inverse quasi fission: studying of the reaction $^{156}Gd + ^{186}W$

The previously model was successfully used for a quantitative description of available experimental data on the previously measured reaction. Beginning to describe an inverse quasi fission example process.

This theoretical study proposes that proton and neutron flow depend on the shell structure of the multidimensional potential energy surface and the values of fundamental parameters that guide the nuclear dynamics, in the lead region increases the yield of target-like fragments formed in the reaction $^{160}Gd + ^{186}W$.

Starting to analise, using the NRV code, we can show the potential energy in function of mass fragment, see the Fig.7, the upward arrows indicate the projectile and the target masses, whereas the downward arrows are referred to the minima potential energy caused by the proton shells at $Z = 28$ and $N = 82$. This configuration corresponds to a fragment of a mass around $200u$ and an exit channel mass asymmetry larger than one of the entrance channel.
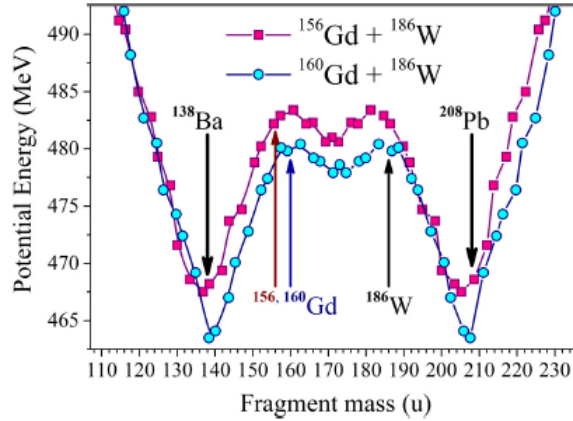

Figure 7: Simulation with the code NRV about the reaction $^{156,160}Gd + ^{180}W$ of the potential energy in function of fragment mass.

The deep minima in the potential energy surface that correspond to the $^{138}Ba + ^{208}Pb$ fragments configuration is due to the influence of the neutron ($N = 82, 126$) and proton ($Z = 82$) at shell closure. As follows from the theoretical calculations, at energies near the Coulomb barrier, shell effects can lead to the considerable enhancement of the yield of reaction products with transfer of up to twenty nucleons.

Studying the reaction $^{156,160}Gd + ^{186}W$, with two beam ions respectively of $878MeV$ and $860MeV$ which strike a layer of $150\mu g/cm^2$ ^{186}W (99.9% enriched) deposited on $50\mu g/cm^2$ carbon backing. Beam intensity on target is 20nA. In the two-body coincidence method are detected two products in coincidence using the two-arm time-of-flight spectrometer CORSET. Start detectors were placed at a distance of 3.5 cm from the target. The acceptance of the spectrometer was $\pm 10°$ in the reaction plane. The angular resolution of the stop detectors is 0.3°.

Through the conservation laws we calculate in the centre-of-mass system of reaction products the primary masses, velocities, angles and energies considering that the mass of the composite system is given as $M_{projectile} + M_{target}$.

Subsequently, is shown in figure 8 Mass-TKE (total kinetic energy) distributions of primary binary fragments in function of the energy near the Coulomb barrier.
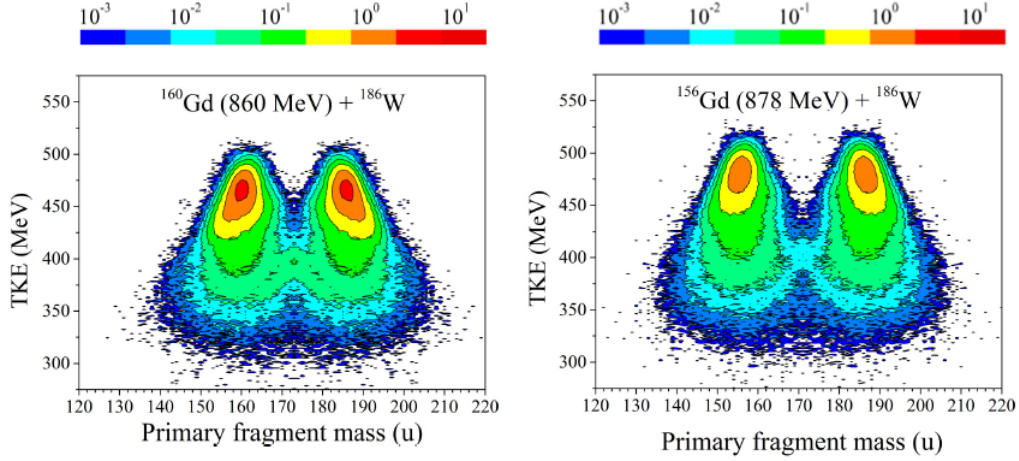
Figure 8: Mass-energy distributions of the primary binary fragments obtained in the reactions $^{156,160}Gd + ^{186}W$ at collision energies 878 MeV and 860 MeV.

This suggests that besides the elastic and quasi-elastic components, a significant part of events has a large dissipation of the initial kinetic energy which indicates the presence of strongly damped collisions.

Furthermore, it can be noted another interesting distribution describing the total kinetic energy lost TKEL ($= Ec.m. - TKE$) for TLF events (shown in Fig 9). Here we can divide the graphic into two parts, lower TKEL values correspond to quasi-elastic processes, whereas higher TKEL values correspond to more damped events. If we use a Gaussian curve to reasonably consider, the quasi-elastic component we observe that most of the damped events are localized at TKEL values above 25 MeV. If we want the cross section σ_R^{exp} of the damped events we can integrate the energy distribution after that we have removed the quasielastic component.
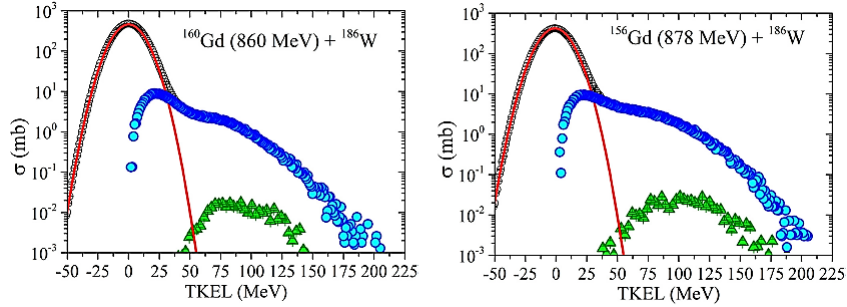

Figure 9: .TKEL distributions of the $^{156,160}Gd + ^{186}W$ reactions for the collision energies of 878 and 860 MeV.

How we can see in the Fig.9, the maximum TKEL is about 175 MeV for the ^{156}Gd with an average of $103 \pm 3 MeV$ and 140 MeV with an average of $92 \pm 3 MeV$ for the ^{160}Gd.

Here the main channel of de-excitation is the neutron evaporation, and if we want to study new heavy isotopes through this process, will be important to know the cross sections of the fragments after the de-excitation. Thus, In Fig.10 are shown the angular distributions of the fragments with mass above 200 u, where we can see a feature of deep-inelastic collisions corresponding to the maximum cross section of the fragments peaks.
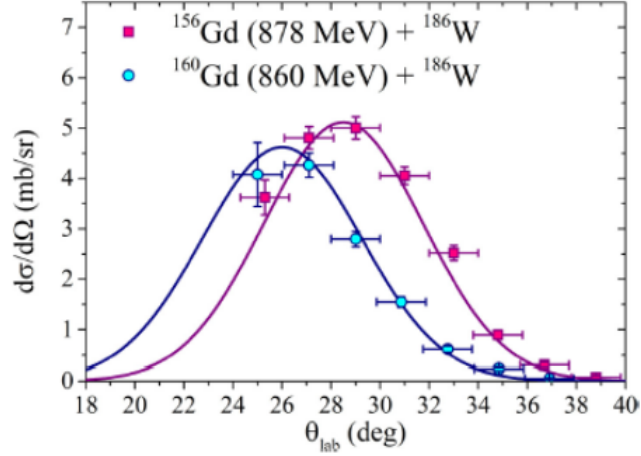
11

Figure 10: Laboratory angular distributions of the reactions $^{156,160}Gd +^{186} W$

Instead, in Fig. 11 there are the mass distributions of heavy binary fragments of the reactions in exam. Here, we have a deviation, corresponding to the shell closure $N = 126$, from the exponential dependency in the region with $A > 200u$ and the mass distributions of heavy primary fragments with $TKEL > 50MeV$ to remove most of the quasielastic events.
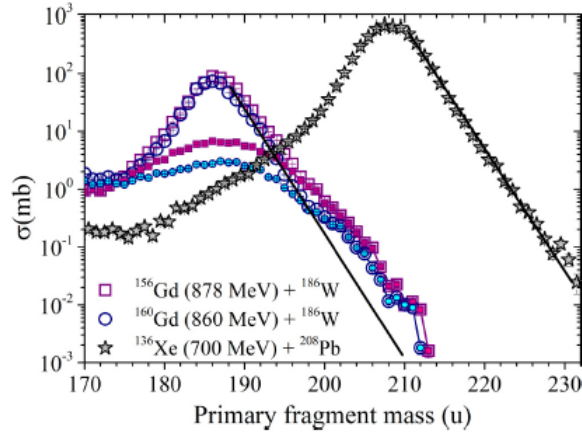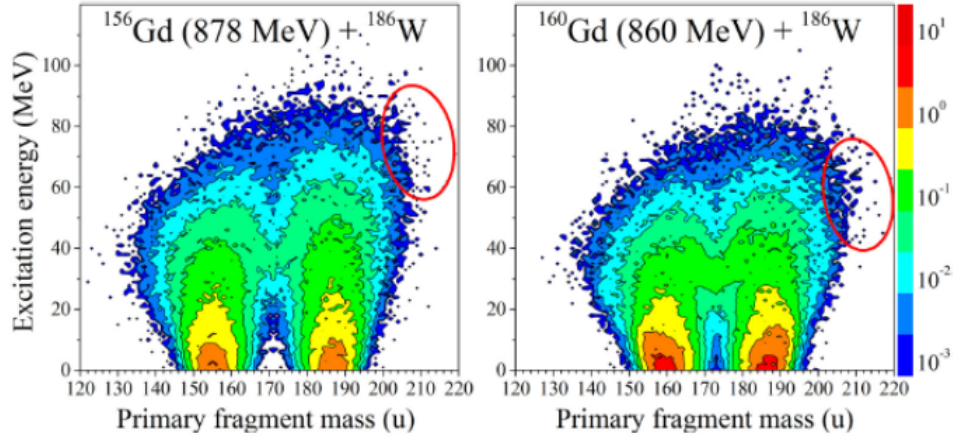

Figure 11: Mass distributions of all primary binary fragments (open symbols) and for events with energy losses more than 50 MeV (filled symbols) for the reactions 156,160Gd + 186W at Elab = 878 (squares) and 860MeV(circles). Mass distributions of primary binary fragments formed in the reaction 136Xe + 208Pb at Elab = 700MeV (stars).

To conclude this discussion, we show the excitation energy of the fragments. This is given as

$$E_f^* = E_{c.m.} - TKE - Q_{gg}$$

and it is proportionally divided between two fragments masses. These quantities are shown in Fig.12 and in the case of $^{160}Gd +^{180} W$ it is present a low neutron evaporation from the fragments, obtaining new neutron-rich nuclei.[9]
.

Abstract

Figure 12: Excitation energy of primary fragments formed in the reactions $^{156,160}Gd +^{186}W$ at collision energies of 878 and $860 MeV$, respectively.

4 Conclusions

The multinucleon transfert process seems to be the more appropriate method to investigate heavy and super heavy neutron rich elements which are, near the stability island like the theorical simulation, made by the model (see par 1.2), show us.

Referred to alla processes studied in this report, the inverse quasi fission is the quite useful tool for understanding and analyse the neutron reach super heavy nuclei formation.

Using projectile and target with mass upper to closure shell $N = 126$ e $Z = 82$, thanking to the asymmetric mass distribution, it is possible obtain light fragments near closure shell and heavy fragments with higher Z and N. Consequently, if the examing elements are neutron rich, it can be able obtain major cross section nuclei than previuosly nuclei.

In this report is added the measuring of thickness mylar foil. The used technique compared two emission spectra respectively with and without foil to measure the energy lost with foil presence. The measured value agrees with the expected one. [7]

The CORSET spectrometer allows to measure mass and energy fragments by the TOF arms using the method introduced in par 2.1. In the end the reaction$^{156,160}Gd +^{186}W$, studing to know the inverse quasi fission process is conditioned by the closed proton and neutron shells on the formation of reaction product. The enhanced yield of products with masses 200–215 u (mass transfer of 20–25 nucleons) was observed for both reactions $^{156,160}Gd +^{186}W$ at energies near the Coulomb barrier for interaction of spherical nuclei.

Although the formation cross sections of these fragments are approximately the same for both reactions, in the case of the ^{160}Gd-induced reaction the excitation energy is 10–20 MeV lower than in the case of ^{156}Gd. It leads to a lower number of neutrons emitted during the de-excitation process in the former reaction. Thus, the reaction with ^{160}Gd ions is more suitable for producing neutron-rich nuclei in the inverse QF process.

References

[1] V. I. Zagrebaev and Walter Greiner physical review c 87, 034608 (2013)

[2] V.I. Zagrebaev tours symposium on nuclear physics v: Tours 2003, AIP Conference Proceedings 704, 2004, 31-40

[3] Mihir B. Chatterjcc Saha Institute of Nuclear Physics 1/AF Bidhannagar Calcutta-700 064

[4] E. M. Kozulin, E. Vardaci, G. N. Knyazheva, A. A. Bogachev, S. N. Dmitriev, I. M. Itkis, M. G. Itkis, A. G. Knyazev, T. A. Loktev, K. V. Novikov, E. A. Razinkov, O. V. Rudakov, S. V. Smirnov, W. Trzaska, and V. I. Zagrebaev physical review C 86, 044611 (2012)

[5] V.V. Saiko, A.V. Karpov acta physica polonica B Vol. 49 (2018)

[6] A. V. Karpov and V. V. Saiko physical review C 96, 024618 (2017)

[7] E. M. Kozulin, A. A. Bogachev, M. G. Itkis, I. M. Itkis, G. N. Knyazheva, N. A. Kondratiev, . Krupa, I. V. Pokrovsky, and E. V. Prokhorova ISSN 0020-4412, Instruments and Experimental Techniques, 2008, Vol. 51, No. 1, pp. 44–58.

[8] H. W. Schmitt, W. E. Kiker, and C. W. Williams physical review volum e 137, number 48 (1965)

[9] E. M. Kozulin, V. I. Zagrebaev, G. N. Knyazheva, I. M. Itkis, K. V. Novikov, M. G. Itkis, S. N. Dmitriev, I. M. Harca, A. E. Bondarchenko, A. V. Karpov, V. V. Saiko, and E. Vardaci physical review C 96, 064621 (2017)